www.czasopisma.pan.pl PAN POLSKA AKADEMIA NAUK www.journals.pan.pl

Arch. Metall. Mater. **62** (2017), 1, 11-17

DOI: 10.1515/amm-2017-0002

A. CIAS*#, M. STOYTCHEV**

NICKEL AND COPPER-FREE SINTERED STRUCTURAL STEELS CONTAINING Mn, Cr, Si, AND Mo DEVELOPED FOR HIGH PERFORMANCE APPLICATIONS

In an attempt to study the sinterability of potential high-strength nickel-free sintered structural steels containing Mn, Cr, Si and Mo compacts were prepared based on sponge and water atomised iron powders and on Astaloy prealloyed powders. To these were admixed ferromanganese, ferroslicon, and graphite. The samples were sintered at temperatures 1120 and 1250°C in laboratory tube furnaces in hydrogen, hydrogen-nitrogen atmospheres with dew points better than –60°C or in nitrogen in a semiclosed container in a local microatmosphere. After sintering the samples were slowly cooled or sinterhardened. Generally resultant microstructures were inhomogeneous, consisted of pearlite/ bainite/martensite, but were characterised by an absence of oxide networks. Sintering studies performed over a range of compositions have shown that superior strength, ranging beyond 900 MPa, along with reasonable tensile elongation, can be achieved with these new steels.

Keywords: sintered steels, alloying elements, sintering atmospheres

1. Theoretical considerations of processing

Alloys for structural powder metallurgy (PM) parts traditionally have been essentially medium carbon low alloy steels containing either or both copper and nickel, with relatively easily reducible oxides, and often additionally some of the more expensive molybdenum. Since (elemental) Ni is carcinogenic [1] and Cu prevents steel recycling, it is worthwhile to investigate Cr and Mn rich compositions. The processing drawbacks associated with oxidation of these elements can be solved by sintering in hydrogen rich atmospheres [2-5], and/or in semiclosed containers. Silicon has an even higher affinity for oxygen than Cr and Mn, so Si PM steels are extremely difficult to process [6-8].

In the multicomponent PM low alloy structural steels, alloying elements, except Cu, are found in solution in iron, in carbides, or as oxides and other non-metal inclusions. Copper dissolves in a-iron at normal temperatures up to 1.0 wt. % and >7%, remains as metal inclusions. It segregates at the graphite/ metal interface and creates, at the sintering temperature, a thin liquid films between the graphite particles and the matrix.

Cr, Mo and Si can form oxides when the sintering atmosphere does not satisfy the Ellingham-Richardson requirements. When added to a semiclosed container, however, such elements as Mn, Al, Si, C deoxidise the steel by taking oxygen from the microatmosphere [8-9] forming MnO, Al_2O_3, SiO_2, CO_2 oxides. Additionally Cr and Mo have greater affinity for carbon than iron, and thus form alloy carbides, replacing cementite. In Cr-Mn steels the alloy carbide $(Cr, Mn, Fe)_{23}C_6$ is formed instead of pure chromium $Cr_{23}C_6$. Cr and Mn alloying elements with high oxygen and carbon affinity have a considerable influence on kinetics and transformation mechanisms in undercooled austenite. Silicon, a noncarbide-forming element, can indirectly influence the thermodynamic activity of other elements during carbide formation.

The majority of Cu, Ni and Mn PM steels are made from mixtures of elemental, partially prealloyed, and diffusion bonded powders, or ferroalloy powders, whereas Mo and Cr steels are normally made from fully prealloyed powders. Mo and Cr, dissolved in iron, do not impair compressibility of steel powders and allow compaction of fully prealloyed powders. Fine (~5 um) Mn-Cr-Mo-(V)-C master alloy additions have been attempted [10], but this was abandoned due to excessive die wear.

In 2-4% Mn steels Cias et al. [11] eliminated continuous manganese oxide networks through careful control of the dew point and/or use of high temperature sintering and semiclosed container. Property variability in Fe-3Mn-0.8C sinterhardened structurally inhomogeneous steel was quantified using Weibull statistics [12]. Sintering in the alpha phase was minimised and, to avoid/minimise formation of oxide veins, was in a dry hydrogen-rich atmosphere. With the use of computer-generated phase diagrams [13], further alloying with Mo, Cr and Si [8] was investigated – with beneficial effects on mechanical properties of Cr and Mo [14]. Bainitic, martensitic and pearlitic structures were concurrently obtained and heat treatments developed. Investigations were conducted re large carbon additions, liquid phase sintering, spheroidisation and warm processing [15-17].

* AGH-UST, UNIVERSITY OF SCIENCE AND TECHNOLOGY, AL. MICKIEWICZA 30, 30-059 KRAKÓW, POLAND.
** INSTITUTE OF METALS SCIENCE, EQUIPMENT AND TECHNOLOGIES, BULGARIAN ACADEMY OF SCIENCES, SOFIA 157467 "SHIPCHENSKI PROHOD" STR., BULGARIA
# Corresponding author: cias@agh.edu.pl

Reported were densities in excess of 7.75 gcm^{-3}, tensile strength of 950 MPa, and strains up to 16% [13, 16] and, through subsequent powder forging [18], increased density, finer spheroidisation and strains in excess of 20%.

This paper considers compositional and processing variables and goes on to consider sinter-hardening.

2. Experimental procedure

The starting powders were: Höganäs: sponge iron NC 100.24, water atomised iron ASC 100.29 and ABC 100.30, Astaloy Mo: Fe-1.5%Mo, Astaloy 85Mo: Fe-0.85%Mo, Astaloy CrL: Fe-1.5Cr-0.2Mo, Astaloy CrM: Fe-3Cr-0.5Mo, Elkem II 77%Mn, 1.3%C, 0.4%Si, 1.5%O, milled and separated in dust extractor to < 20 μm, Elkem S 87,6%Mn, 1.0%C, 0.46 O, milled and sieved to < 40 μm, Huta Pokoj (HP II) 73%Mn, 6.3%C, 0.7%Si, 1.3%O, milled and sieved to < 40 μm, OFZ Istebné type 44.0 Fe-45%Si, particle size <20 μm and C-UF ultra fine pure graphite (AGH) and Trimex F10 (IMS).

Specimen batches are designated AGH and IMS, relating to sites of experiments: AGH, Krakow, and IMS BAS, Sofia, respectively. Powders were mixed in double cone mixer (AGH) and drum ball mixer (IMS). The nominal compositions are given in Table 1.

TABLE 1

Compositions of the powder mixtures and their sintering temperatures

Sample	Nominal composition, wt %	Formulation	Sintering temperature,°C	Sintering atmosphere
AGH 1	Fe-3Mn-0.8C	NC100.24 + HP II + graphite	1120	H_2
AGH 2		ABC100.30 + HP II+graphite	1120 and 1250	
AGH 3		NC.100.24 + Elkem II+ graphite		H_2, semiclosed container
AGH 4				N_2, semiclosed container
AGH 5	Fe-3Mn-0.6C-0.5Mo	Astaloy 85Mo + NC100.24 + HPII + graphite		H_2, semiclosed container
AGH 6	Fe-3Mn-0.8C-0.5Mo		1250	
AGH 7	Fe-4Mn-0.6C-0.5Mo		1120 and 1250	
AGH 8	Fe-4Mn-0.8C-0.5Mo			
AGH 9	Fe-1.5Mn-1.5Cr-0.25Mo-0.4C	Astaloy CrL+ Elkem II + graphite	1120	H_2, semiclosed container
AGH 10				N_2, semiclosed container
AGH 11	Fe-3.2Mn-1.4Si-0.5C	NC 100.24 + Elkem II + ferrosilicon Fe-45%Si + graphite	1120 and 1250	N_2, semiclosed container + ferromanganese + Al + naphtalene + NH_4I + Na_2CO_3 (local microatmosphere)
AGH 12	Fe-3Cr-0.5Mo-0.6C	Astaloy CrM + graphite	1120 + 200°C 1h	
AGH 13	Fe-3Cr-1Mn-0.5Mo-0.4C	Astaloy CrM + Elkem II + graphite	1250 + 200°C 1h	H_2, semiclosed container
IMS 1	Fe-3Mn-0.6C	ASC100.29 + Elkem S + Mo + graphite	1280	75%H_2-25%N_2
IMS 2	Fe-3Mn-0.85Mo-0.6C			
IMS 3	Fe-3Mn-1.5Mo-0.6C			
IMS 4	Fe-3Mn-0.6C			
IMS 5	Fe-3Mn-0.85Mo-0.6C			
IMS 6	Fe-3Mn-1.5Mo-0.6C			

Primary sinterability data were obtained using a horizontal dilatometer NETZSCH 402E. The specimens were uniaxially compacted at ~500 MPa in a special 15×4×4 mm^3 rectangular die to densities in the range of 6.1-6.5 g/cm^3. Temperature was raised to 1250°C for varying sintering times under dynamic pure hydrogen atmosphere with dew point better than –60°C. The powder mixtures were compacted at 500-660 MPa into standard dogbone tensile specimens conforming to ISO 2740/MPIF standard 10 and into rectangular transverse rupture strength (TRS) specimens, 55×10×5 mm^3. The green densities were in the range 6.5-7.25 gcm^{-1}. At AGH zinc stearate was used for die wall lubrication and Kenolube addition was made in IMS.

Sintering in laboratory furnaces for 1 hour was at 1120 and 1250°C in hydrogen and technical nitrogen atmospheres with –60°C dewpoint at AGH, and at 1280°C, in 75H_2/25N_2 atmosphere with –65°C dewpoint at IMS. AGH specimens were sintered in a semiclosed container, containing sometimes Al, ferromanganese powder (getter – an oxygen binder), naphthalene as well as activator: NH_4I, and Na_2CO_3 (Table 1). These compacts were simultaneously sintered with a ferromanganese lump or powder (~15 g, Elkem Fe-77%Mn-1.3%C – the donor of manganese), and/or solid naphthalene ($C_{10}H_8$, the donor of carbon) placed additionally in the container with a small amount of ammonium iodide (NH_4I) and sodium carbonate (Na_2CO_3) as activators/energizers using the methodology described elsewhere [9,19]. The microatmosphere had sufficient manganese (an oxygen binder) for "self-cleaning", "gettering", and nascent carbon to minimise/avoid the loss of carbon from the compacts [8,20]. For AGH specimens the gas flow was ~0.2 cm^3 min^{-1} per cm^2 of furnace tube cross sectional area. Cooling rates ranged from 7 (all IMS) to 65°C min^{-1} (AGH sinterhardened specimens). The sinterhardened specimens were subsequently tempered at 200°C for 1 hour.

Chemical analyses for oxygen, nitrogen and carbon in the starting powders and in the sintered alloys, measured on at least

3 specimens, were carried out according to ASTM E 1019-2 on Leco apparatus: TC-336 and CS-125, respectively and Tables 2-4 list the sintered compositions.

TABLE 2

Chemical analyses of sintered Fe-4Mn-0.8C-0.5Mo (AGH 8)

Sintering temperature,°C	Cooling rate, °C min^{-1}	Chemical analyses wt. %			
		Mn	C	O	Fe
1120	1.5 (furnace cooling)	3.85	0.658	0.201	Bal.
1250	1.5 (furnace cooling)	3.75	0.496	0.130	Bal.
1250	60	3.71	0.532	0.162	Bal.

TABLE 3

Chemical analyses of sintered Fe-1.5Mn-1.5Cr-0.25Mo-0.4C (AGH 9 and 10)

Sintering conditions: 1120°C, 60 min.	Cooling rate,°C min^{-1}	Chemical analyses wt. %		
		C	O	N
H_2	60	0.445	0.401	0.00395
N_2		0.412	0.380	0.0444

TABLE 4

Chemical analyses of sintered Fe-3.2Mn-1.4Si-0.5C (AGH 11)

Sintering conditions:	Cooling rate, °Cmin^{-1}	Chemical analyses, wt. %		
		C	O	N
N_2,1120°, 60 min., ferromanganese + naphtalene + NH_4I + Na_2CO_3	60	0.288	0.51	0.0269
N_2,1250°, 60 min., ferromanganese + naphtalene + NH_4I + Na_2CO_3		0.253	0.54	0.0753

Density, apparent hardness, and tensile properties were determined according to ISO 2740 and MPIF Standards 43, 44 and 10, respectively. For metallographic investigations on a Leica DMLM optical microscope, the samples were mounted in bakelite, polished and etched in Nital (3 wt.% HNO_3-97 wt.% H_2O). Fractographic examinations were carried out in a Zeiss Merlin FE-SEM (field emission scanning electron microscope) equipped with EDS Quantax 830 and EBSD Quantax CrystAlign 200 system.

3. Results

Dilatometry indicated that the optimum composition range for dimensional stability was between 2 and 4% Mn (Fig. 1).

With addition of 0.6-0.8% carbon it was possible to balance the composition and sintering regime such that no high dimensional change takes place and tensile strength is maximum. Except for the alloy containing 1.4% silicon (AGH 11), there was no significant dimensional change in any of the specimens, Tables 5 and 6, which also list mechanical properties.

Insignificant plasticity was present in the relatively low green density specimens. For higher green density materials,

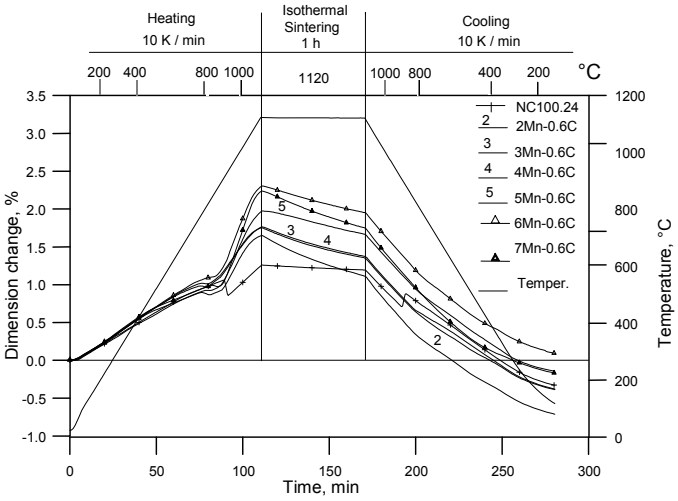

Fig. 1. Dilatometric traces for NC100.24 + HP II ferromanganese Fe-(2-7)Mn-0.6C specimens isothermally sintered 1 hour at 1120°C in hydrogen

increased tensile elongation, resulting from tempering at 200°C, with only ~10% strength loss, is to be noted. The beneficial effect on mechanical properties of the sintering in microatmosphere with getter and activator is shown in Table 5.

Pearlitic transformation in all the investigated alloys is slower than in the classical iron-carbon system and manganese-containing austenite is far more stable with respect to transformation to martensite. Only very slow furnace cooling (3.5°C/min) from the sintering temperature produced lamellar pearlitic microstructures, which were usually initiated at pores present during sintering. In the convective fast cooled (65°C min^{-1}) condition microstructures consisted of bainite and martensite with some retained austenite. The convectively medium (~7 and 10°C min^{-1}) cooled specimens showed a more heterogeneous microstructure consisting of pearlite, upper and lower (coarse and fine) bainite, martensite, retained austenite and in some cases residual ferritic cores of the iron powder particles. Only when the base powder was atomised iron and sintering temperature 1120°C, islands of troostite and bainitic/martensitic rims were found around ferrite areas. This is due to the poorly distributed manganese, whose concentration decreases towards the centres of the iron powder particles. Carbon was retained in the Mn-rich areas, and interiors of the particles were thus partly ferritic. Faster Mn diffusion and thus better microstructural homogeneity was achieved by sintering at higher temperatures and by using sponge iron powder. In alloys sintered at 1250°C Mn alloyed zones grew deeply into the Fe particles, and bainitic/martensitic rims were not present in most of the iron powder particles.

The amounts of bainite and martensite increased significantly at the higher cooling rate, thus resulting in increasing apparent cross-section hardness. The microstructures of Mn and Cr steels contained significant portions of pearlite when slow cooled. In the Mo containing alloy a large amount of lower bainite was found for the medium (~10°C/min) cooled state. Fast cooled Mn steels (65°C min^{-1}) contained significant amounts of retained austenite.

TABLE 5

Properties of Mn steel specimens: as-sintered and cooled at AGH at 60°C min^{-1}

Sample	Nominal composition	Sintering temperature,°C	Sintered density, gcm^{-3}	Dimensional change, %	Apparent hardness, HV30	Tensile strength, MPa	Strain to failure, %
AGH 1	Fe-3Mn-0.8C	1120	6.8	+0.33	217	516	< 1
AGH 2		1120	6.8	+0.28	214	491	< 1
AGH 3		1120	6.8	+0.35	216	633	1.3
		1250	6.8	–0.43	233	724	1.1
AGH 4		1120	6.8	–0.1	212	651	1.4
		1250	6.8	+0.25	233	776	1.4
AGH 5	Fe-3Mn-0.6C-0.5Mo	1120	6.7	+0.3	273	460	< 1
		1250	6.8	–0.2	315	596	< 1
AGH 6	Fe-3Mn-0.8C-0.5Mo	1120	6.7	+0.4	281	451	< 1
		1120 + temper 200° 1h	6.7	+0.4	256	450	1.2
		1250	6.8	0.0	324	531	< 1
		1250 + temper 200° 1h	6.8	0.0	295	570	1.5
AGH 7	Fe-4Mn-0.6C-0.5Mo	1120	6.7	+0.3	262	383	< 1
		1120 + temper 200° 1h	6.7	+0.3	293	560	1.1
		1250	6.8	–0.1	316	416	< 1
		1250 + temper 300° 1h	6.8	–0.1	341	610	1.7
AGH 8	Fe-4Mn-0.8C-0.5Mo	1120	6.7	+0.4	255	283	< 1
		1250	6.8	+0.1	314	319	< 1
AGH 9	Fe-1.5Mn-1.5Cr-0.25Mo-0.4C	1120	6.5	–0.66	197	586	0.6
AGH 10			6.5	–0.62	215	633	0.9
AGH 11	Fe-3.2Mn-1.4Si-0.5C	1120	6.6	0.19	254	783	2.2
		1250		–0.51	291	871	2.2
AGH 12	Fe-3Cr-0.5Mo-0.6C	1120	6.9	–0.1	380	908	3.2
AGH 13	Fe-3Cr-1Mn-0.5Mo-0.4C	1250 + 200°C 1h	7.0	+0.1	301	840	2.5

Mechanical properties, Table 5, were not only related to microstructure, but also to the size, distribution, and morphology of porosity and oxide inclusions, generally consisting of $MnO\text{-}Al_2O_3\text{-}SiO_2$ compounds. In all the specimens the segregation of Mn and Si to grain boundaries, perhaps in the form of MnO and SiO_2, is believed to degrade the bond strength. This is consistent with the observed intergranular cracking due to the weakened grain boundaries. Only steel AGH 12, the microstructure of which is illustrated in Fig. 2, emanating from compacts sintered at N_2 in the semiclosed container + ferromanganese + Al + naphtalene + NH_4I + Na_2CO_3 (local microatmosphere) are there extensive regions of dimple rupture, shown in Fig. 3, which indicates that then the grain/interparticle boundaries were more failure resistant.

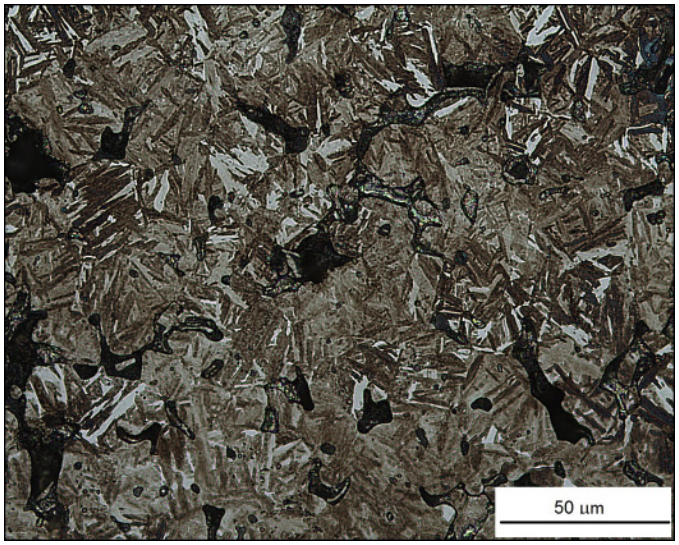

Fig. 2. Microstructure of specimen AGH 12 (0.59%C) comprising, in somewhat varying proportions, upper and lower bainite, martensite and retained austenite; note the absence of chromium oxide networks

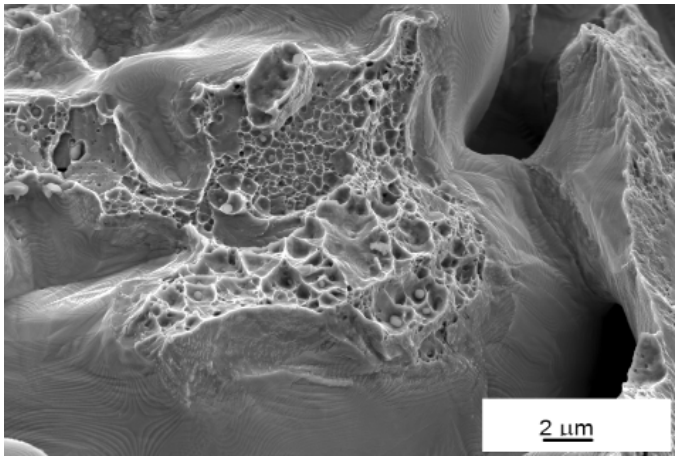

Fig. 3. Fractograph of specimen AGH 12 comprising dimple ductile facets with localised plastic deformation (relating principally to microvoid coalescence in sinter necks) and dimple rupture/transgranular fracture surfaces with isolated or clustered carbide inclusions, indicating that grain/interparticle boundaries were more failure resistant, i.e. not degraded by (thin) oxide films

4. Discussion

In Fe-3Mn-0.8C steel sintered in wet hydrogen atmosphere discrete intergranular MnO particles were formed deep in the alloy beneath bands of oxides which developed over intersections of grain boundaries with the surface, or beneath grain-boundary oxides near the surface [21]. One process developed to suppress oxidation of steels with high contents of Cr, Si and Mn during sintering in an open boat uses dry, dew points better than –65°C, hydrogen. A shortcoming is that the process does not remove manganese and silicon oxides. When pure nitrogen is the protective gas, in the interior of the semiclosed container (sintering box), reactions of oxygen or oxygen carriers such as CO_2 and H_2O with these element can be prevented [22]. In addition, transport of oxygen and oxygen carriers from the heat-resistant material of the furnace (link belt conveyor, muffle, etc) to the material to be sintered is prevented. The use of nitrogen as the inert gas is to some extent restricted because undesired formation of nitrides at the surface of the material being processed might occur. Adding a chemically active material such as manganese vapour to the sintering microatmosphere draws oxygen from the alloy into Mn oxide particles, which float to the bottom of the sintering boat, where they can be skimmed off, resulting in relatively oxygen-free Cr steel [19]. When ferromanganese powder and Al (thermodynamic activity = 1) and NH_4I, NaCl activators/energizers were additionally introduced into a semiclosed container, the steel was aluminized when the following equilibria pertained [22]:

$$Al_{(l)} + NaCl_{(l)} \leftrightarrow AlCl_{(v)} + Na_{(v)} \quad (1)$$

$AlCl_{2(v)}$ and $AlCl_{3(v)}$ were also formed in the container. The most important reaction occurring on the substrate surface is the dissociation of the metal halide vapours AlCl or $AlCl_2$, e.g.

$$2AlCl_{(v)} \leftrightarrow AlCl_{2(v)} + Al \quad (2)$$

The getter/activator in this local microatmosphere does not only protect the metal against oxidation, but acts also as an aid to remove the oxide skin off the metal and clean the green compact. Aluminium has an even higher affinity for oxygen than manganese, thus, when sintering Cr and Mn steels an intensive oxidation of Al takes place, resulting in the very stable Al_2O_3.

Examination of processing of the Mn(-Mo) steels, on the basis of compositions of the powder mixtures, green density, sintering temperature, dew point [23-26] and the data of Mitchell et al. [17] indicates that green densities of ~6.6 gcm^{-3} are inadequate if high strengths are to be obtained. Increasing the sintering temperature to 1250 or 1280°C, additional to pore rounding and increasing homogeneity (not necessarily desirable), has little effect at these low green densities. Strength increases were of the order of 20% (Table5) over conventional 1120°C sintering. When the 6.8 gcm^{-3} green density was raised to 7 gcm^{-3} by pressing at 800 MPa, by cooling from the 1250°C sintering temperature at 65°Cmin^{-1}, plus tempering 200°C for 1hour, tensile strength of 840 MPa was reproducibly produced, concurrently with 2.5% plastic strain (AGH 13).

Only when liquid phase sintering takes place can further significant improvements in sintered density and mechanical properties be expected. To obtain liquid phase at 1280°C, however, Abosbaia and Mitchell [13,16], used much higher C content, 1.3%. There seems to be no benefit of relatively high Mn contents in PM Mn-Mo-C steels, note the wrought compositions, e.g. 0.38C-1.75Mn or 0.38C-1.5Mn-0.45Mo. The optimisation of PM compositions is likely to be below 2% Mn and 1% Mo, with C determined by end use of the sintered (and heat treated) component. Although the effect of Mo on the hardenability of low alloy steels is well established and commercially exploited in wrought Mn steels, the situation is not yet satisfactorily understood for PM Mn and Mn-Si steels. It is clear, however, that Ni is not as effective as manganese in promoting bainite formation. Cr as a further alloying element deserves further consideration and in this context availability of prealloyed Fe-Mo-Cr, Astaloy CrM, not necessarily of optimum composition for high performance structural parts, should be recalled [27,28].

Tempering of sinterhardened Mn-Mo steels allows a balancing of strength and ductility. For Fe-4Mn-0.6C-0.5Mo alloy (AGH 7) sintered at 1250°C, raising the tempering temperature to 300°C resulted in ductility of 1.7% with a corresponding increase in tensile strength (Table 5). In the absence of Mo, more rapid cooling rates are required for optimum properties after tempering. The optimum convective cooling rate prior to final tempering is then in the range 30-60°C min^{-1}, not readily available in industrial furnaces. As Mn and Mo contents increase, much longer cooling times are needed to obtain large proportions of bainite. Concurrently martensite and retained austenite were detected, in (small) amounts, depending on the cooling rate.

The best combination of mechanical properties of Fe-3.2Mn-1.4Si-0.5C (AGH 11) matched that reported by Klein et al. [6,7], who sintered their specimens in dry hydrogen. In this work sintering was in technical nitrogen in a semiclosed container with additives: ferromanganese lump (source of Mn vapour) and/or solid naphthalene (the donor of carbon) with a small amount of ammonium iodide (NH_4I) and sodium carbonate (Na_2CO_3) as activators/energizers. It is suggested that, after appropriate technology transfer, this process can be economically industrially exploited. A major problem is the unacceptable use, on health and environmental considerations, of naphtalene. Of special relevance are the very encouraging preliminary data [21] regarding sintering in cryogenic nitrogen with aluminium and activator (NaCl).

Thermodynamic driving forces and kinetic factors should dictate the selection of proper alloying elements and the form in which they are to be added for sintering in the local microatmosphere. In the case of Cr, driving forces for the formation of chromium oxide and for the expulsion of this alloying element from the Fe alloy are relevant. The first type corresponds to the standard free energy of oxide formation $\Delta G°$, and can be found in the Ellingham-Richardson diagram. If $\Delta G°$ values of some elements are not available on the diagram, heat formation $\Delta H°$, can be used [29]. If Al, Si, and Mn are in contact with Cr_2O_3, the reduction reaction of Cr_2O_3 allows Cr atoms to migrate into

iron particles. In contrast, such reaction is negligible for metals of moderate $\Delta G°$, which may be preferable as alloying elements.

The second type of the driving force is related to the activity coefficients, γ_s, measures of deviation from a state of ideal solid solution, of alloying elements in Fe, which represent the excess chemical potential. For Cr in the ideal solid solution of Fe-Cr, it is given by:

$$\mu_{Cr} = \mu^0_{\mathrm{Fe}} + RT\ln N_{Cr} \tag{3}$$

Here μ^0_{Fe} is the chemical potential of the pure Fe matrix and N_{Cr} is the concentration of Cr. When there is deviation from the ideal state by chemical interaction, the chemical potential of alloying either increases or decreases with respect to that in Eq. (1). This is given by:

$$\mu_{Cr} = \mu^0_{\mathrm{Fe}} + RT\ln \alpha_{Cr} = \mu^0_{\mathrm{Fe}} + RT\ln N_{Cr} + RT\ln \gamma_{Cr} \tag{4}$$

Here α_{Cr} is the activity and is given by the product of concentration N_{Cr} and activity coefficient γ_{Cr}. The activity coefficient is 1 for the ideal state and larger or smaller for a non-ideal state. When >1, the chemical potential increases from that of the ideal state, which suggests that an alloying element leaves Fe if more stable configurations are available by reacting with a neighbouring phase of the alloy. One such example is the migration of Cr to the Fe-Cr powder particle surface, followed by the formation of Cr oxide in an oxygen-containing atmosphere. In this way, the total free energy of the system O_2-Fe-Cr, including atmosphere and Fe-Cr/Cr_2O_3, can be minimized. In contrast, when the activity coefficient is <1, chemical potential decreases from that of the ideal state and the alloying element tends to remain as a Fe solid solution, unless the first type of driving force is very strong. In this regard, the third term in Eq. (2), $RT\ln\gamma_{Cr}$, is considered as a driving force to expel the alloying element and to make the Fe-Cr alloy transform to pure Fe and Fe-Cr/Cr_2O_3 oxide layer in the presence of oxygen or water vapour containing atmosphere. Another example is migration of Cr to cementite or Fe/graphite interface, followed by the reaction and formation of complex carbide including Cr, e.g. $(Fe, Cr, Mo)_3C$, or carbide Cr_nC_m (Figs. 3 and 4).

5. Conclusions

Efficiency of semiclosed containers to sinter in nitrogen Cr, Mn, and Si steels can be further enhanced by employing as microclimate additives: nascent carbon, manganese vapour and aluminium. Iron powder with a high specific surface area, e.g. Höganäs NC 100.24 sponge iron, should be used to ensure good homogeneity of manganese when sintering Mn-(Mo)-C steels at temperature of 1120°C. To utilise the potential of alloying elements, higher sintering temperatures, around 1250°C, are required, as are green densities higher than 7gcm^{-3}. Thus, when the green density was raised to 6.8 gcm^{-3} by pressing at 660 MPa of Fe-3Mn-0.6C alloy (AGH 4) and cooling from 1250°C at 65°Cmin^{-1}, reproducible tensile strength of 776 MPa and 1.4%

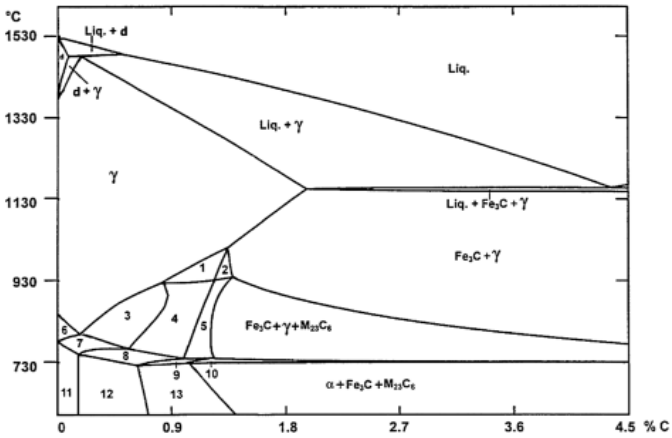

Fig. 4. Computer generated Fe-3Cr-1Mn-0.5Mo-(0-4.5) C equilibrium phase diagram; Fe_3C signifies $(Fe, Cr, Mo)_3C$; **1** – g+M_7C_3; **2** – Fe_3C+g+M_7C_3; **3** – g+$M_{23}C_6$; **4** – g+M_7C_3+$M_{23}C_6$; **5** – Fe_3C+g+M_7C_3+ $M_{23}C_6$; **6** – a+g; 7 – a+g+$M_{23}C_6$; **8** – a+g+ M_7C_3+$M_{23}C_6$; **9** – a+g+Fe_3C+M_7C_3+$M_{23}C_6$; **10** – a+g+Fe_3C+$M_{23}C_6$; **11** – a+$M_{23}C_6$; **12** – a+M_7C_3+$M_{23}C_6$; **13** – a+Fe_3C+M_7C_3+$M_{23}C_6$

plastic strain were achieved. By controlling cooling rate, a variety of phases can be simultaneously obtained, some with appreciable hardenability. Furnace cooling produced significant ductility at the expense of hardness and convective cooling resulted in much higher hardness. The use of iron prealloyed with 0.85 or 1.5%Mo, in place of a part of plain iron, in iron -ferromanganese blends gave improved mechanical properties (AGH 5-8 and IMS 2-6). Mechanical properties (hardness, transverse rupture strength, tensile strength) all show the positive effect of Mo addition to Fe-(3-4) Mn, but lower Mn contents, preferably with Cr addition (AGH 9, 10 and 13), need further investigation. There is also potential for developing tempered structures combining strength and toughness in sinterhardened alloys (AGH 12 and 13), as well as Fe-Mn-Si alloys sintered in a local microatmosphere with getter and activator, (AGH 11).

Acknowledgements

This work was sponsored by the Polish Ministry of Science and Higher Education under Contract no. 11.11.110.299. Appreciation is also expressed to Prof. A. S. Wronski for his advise and comments, as well as editing the manuscript.

REFERENCES

[1] EU Carcinogen Directive 2004/37/EC of 29 April 2004 – carcinogens or mutagens at work.

[2] E. Hryha, E. Dudrova, L. Nyborg, Metall. Mater. Trans. A **41A**, No. 11, 2880 (2010).

[3] L.S. Sigl, P. Delarbre, in: Adv PM Part, MPIF (Ed.), Princeton, NJ, part 7, 54 (2003).

[4] H. Danninger, Chen Xu, B. Lindqvist, Mater. Sci. Forum **534-536**, 577 (2007).

[5] T. Pieczonka, M. Sułowski, A. Ciaś, Arch. Metall. Mater. **57**, 4, 1001 (2012).
[6] A.N. Klein, R. Oberacker, F. Thümmler, Powder Metall. Int. **17**, 2, 71 (1985).
[7] A.N. Klein, R. Oberacker, F. Thümmler, Powder Metall. Int. **17**, 1, 13 (1985).
[8] A. Cias, Int. J. Mater. Res. **106**, 5. 494 (2015).
[9] A. Cias, Sci. Sinter. **45**, 379, (2013).
[10] F. Lenel: Powder Metallurgy, Principless and Applications. Metal Powder Industries Federation, Princeton, MY 1980, p. 416.
[11] A. Ciaś, S. C. Mitchell, A. Watts, A. S. Wronski, Powder Metall. **42**, No 3, 227 (1999).
[12] A. Ciaś, A. Czarski, Arch. Metall. Mater. **58**, 4, 1045 (2013).
[13] A. S. Abosbaia, S. C. Mitchell, M. Youseffi, A. S. Wronski, Powder Metall. **54**, 5, 592 (2011).
[14] M. Sułowski, Ciaś A., Arch. Metall. Mater. **56**, 2, 293 (2011).
[15] R.J. Causton and T. M. Cimino, in: Adv PM Part, MPIF (Ed.), Princeton, NJ (1994). NJ, presented at 1994 Int. Conf. & Exhibit. on PM & Part. Mat., May 8-11, 1994 – Toronto, Canada.
[16] S.C. Mitchell, M. Youseffi, A. S. Abosbaia, J. Ernes, Powder Metall. Progress **8**, 2 , 91 (2008).
[17] S.C. Mitchell, S. Szczepanik, P. Nikiel, A. S. Wronski: Rudy i Metale Nieżelazne **59**, 12, 605 (2014).
[18] S. Szczepanik, S. C. Mitchell, A. A. S. Abosbaia, A. S. Wronski, Powder Metall. Progress **10**, 1, 59 (2010).
[19] A. Cias, Powder Metall. **56**, 3, 231 (2013).
[20] A. Cias, Sci. Sinter 47, 1, 61 (2015).
[21] A. Cias, Kovove Mater., **54**, 4, 269 (2016).
[22] A. Ciaś: Development and properties of Fe-Mn-(Mo)-(Cr)-C sintered structural steels, ISSN0867-6631, 129, AGH - UWNT, Kraków 2004.
[23] A. Cias , M. Sułowski, Arch. Metall. Mater. **54**, 4, 1093 (2009).
[24] M. Sułowski, A. Ciaś, M. Stoytchev, T. Andreev, Mater. Sci. Forum **534-536**, 753 (2007).
[25] M. Sułowski, A. Ciaś, H. Frydrych, J. Frydrych, I. Olszewska, R. Goleń, M. Sowa: Mater. Sci. Forum **534-536**, 757 (2007).
[26] A. Ciaś, A.S. Wroński, Powder Metall. **53**, 4, 328 (2010).
[27] E. Hryha, L. Nyborg, E. Dudrova, S. Bengtsson, Proc. of World Congress & Exhibit. PM2010, **3**, 87 (2010). ISBN/ISSN: 9781899072125
[28] E. Hryha, E. Dudrova, T. Mizutani, Application of Thermodynamics to biological and materials science, chapter 22, p. 573 (2011). ISBN: 978-953-307-980-6
[29] Smithells Metals Reference Book, 7th ed., E. A. Brandes and G. B. Brook, eds. Butterworth Heinemann (1992).